PHYSICAL REVIEW C VOLUME 8, NUMBER 3 SEPTEMBER 1973

# Nuclear Scattering of Plane-Polarized Photons

Evans Hayward
*National Bureau of Standards, Washington, D.C. 20234*

W. C. Barber*
*Massachusetts Institute of Technology, Laboratory for Nuclear Science, Cambridge, Massachusetts 02139*

Jed Sazama†
*Harry Diamond Laboratories, Washington, D.C. 20438*
(Received 9 May 1973)

A beam of plane-polarized monochromatic photons has been produced by the resonance fluorescence of the well-known $1^+$ state at 15.1 MeV in $^{12}C$. These have been scattered a second time from natural targets of Cd, Sn, Ta, W, Pt, Au, and Bi. Measurements were made with poor energy resolution of the relative number of photons scattered at 90° parallel and perpendicular to the polarization vector in the incident 15.1-MeV beam. The observation of photons scattered along the polarization vector reflects the contribution of incoherent scattering to the dominant coherent-scattering process and results either from permanent nuclear deformation or from the dynamic deformation produced by the coupling of the giant dipole resonance with the quadrupole oscillations of the nuclear surface. The observed intensities of incoherent scattering are of the same order of magnitude for the deformed nuclei and the spherical vibrators and agree roughly with the predictions of the dynamic collective model. No incoherent scattering was observed from the rigid sphere $^{209}Bi$.

## I. INTRODUCTION

The tensor character of the nuclear polarizability was first observed[1-3] in connection with photon scattering by the deformed nuclei Ta, Ho, and Er. The scattering cross section was shown to possess the usual coherent part, which is related to the absorption cross section through the optical theorem and the dispersion relation, plus an additional incoherent part that populates those members of the ground-state rotational band that can be reached in electric dipole transitions from the giant resonance. At that time the nuclear polarizability from a spherical nucleus was assumed to be a simple scalar because there was nothing in the data to deny it.

A few years later Danos and Greiner,[4] Le Tourneux,[5,6] Semenko,[6-8] and Kerman and Quang[9] pointed out that the oscillating nuclear surface might couple to the electric dipole mode and produce changes in the structure of the giant resonance. In this model, called the dynamic collective model, the giant resonances of the spherical nuclei acquired several peaks. Indeed, peaks ascribed to this effect have been reported by several authors.[10-14] For the deformed nuclei, the upper resonance state was actually split into two and each of the three resonances had a satellite associated with it. However, when appropriate widths were folded into these states, the giant-resonance cross section remained very similar to that predicted by the simple two-resonance picture.[15]

Since the coupling of the giant resonance with the nuclear surface oscillations implies that the giant-resonance scattering cross section has components that populate those low-lying vibrational states that can be reached in electric dipole transitions, the observation of these deexcitation photons represents a direct test of the basic concept of the dynamic collective model. These photons have perhaps already been observed in an experiment[16] in which the giant resonance was excited with 32-MeV bremsstrahlung and the NaI(Tl) pulse-height distribution, generated by the scattered photons, interpreted. The object of the experiment described in this paper was to make a more direct observation of these deexcitation photons.

The present experiment was conceived[17] several years ago and typical results to be expected were predicted on the basis of the dynamic collective model. The central idea is to excite the giant resonances of heavy nuclei with the monochromatic photons produced by the resonance fluorescence of the 15.1-MeV $1^+$ state in $^{12}C$. This level has a large ground-state radiation width and its energy coincides with the giant resonances of the medium and heavy nuclei. Since the 15.1-MeV radiation scattered at 90° is plane polarized, a measurement of the azimuthal angular distribution of photons scattered by a second target permits a determination of the angular momentum properties of the states involved in the scattering.

It allows a separation of the scalar and tensor parts of the scattering cross section and tests directly whether the dipole resonance is coupled with the quadrupole oscillations of nuclear surface as is assumed in the dynamic collective model.

## II. EXPERIMENTAL DETAILS

The physical arrangement of the experiment is shown in Fig. 1. The resonance fluorescence source has been constructed in the 8-m-long tunnel orginally intended as a beam dump behind the electron scattering spectrometer. A 20-MeV beam from the electron linear accelerator is steered and focused onto a removable BeO view screen just before the end of the vacuum system. Then, with the view screen out, the electrons are allowed to strike a 0.1-radiation-length-thick tantalum target located about 1 cm beyond the end of the vacuum system. The electrons are then bent downward into a water-filled electrically isolated beam dump; the integrated beam-dump current serves as a monitor. A second magnet located before the tantalum radiator cancels the fringing field of the dumping magnet so that the electrons are horizontal when they radiate. The current in this magnet is adjusted to equalize the currents from the upper and lower halves of the split ion chamber.

The 4-g/cm$^2$-thick graphite target is centered 25 cm from the radiator almost touching the dumping magnet. The dumping-magnet pole faces are tapered, not only to maximize the field strength where the electrons enter but also to minimize background produced by either electrons or bremsstrahlung scraping them. In this geometry the graphite target intercepts more than 90% of the bremsstrahlung. The 15.1-MeV photons emitted at 90° by the carbon target travel through the 20-cm-diam hole drilled through the 2.4-m heavy concrete wall that separates the tunnel from the service area where the detectors are located. The beam is defined by a series of collimators throughout the wall and is filtered through 10 cm of borated polyethylene and the 1.4 g/cm$^2$ of aluminum that constitute the transmission-ionization chamber. When it reaches the second scatterer the beam has a diameter of about 18 cm and has about 80% of its initial intensity. When 50 $\mu$A of 20-MeV electrons are incident on the tantalum radiator, approximately $10^4$ 15.1-MeV plane-polarized photons/sec are available to strike a second target.

A scattering target of the material under study was placed at the location indicated in Figs. 1 and 2. The target position was viewed by three sodium iodide detectors, 12.7 cm in diameter and essentially 10 cm long; the upper detector is slightly shorter and the lower one slightly longer. Each detector is encased in a lead casket having 12.7-cm-thick walls. Outside of the lead there is at least 30 cm of neutron shielding, paraffin, borax, or borated polyethylene around each detector. Each detector views the target through 22.8 cm of aluminum which removes low-energy photons generated in the target.

The pulses from the photomultiplier anodes were fed directly into wide-band amplifers that were used to drive the 145-m-long cables between the service area and the counting room. There they were further amplified and fed into discriminators and pileup rejection circuits that eliminated pulses that were distorted on the leading edge. The pulses were then amplified and shaped using conventional commercial circuits and finally analyzed by 64-channel pulse-height analyzers. The latter were gated on 360 times

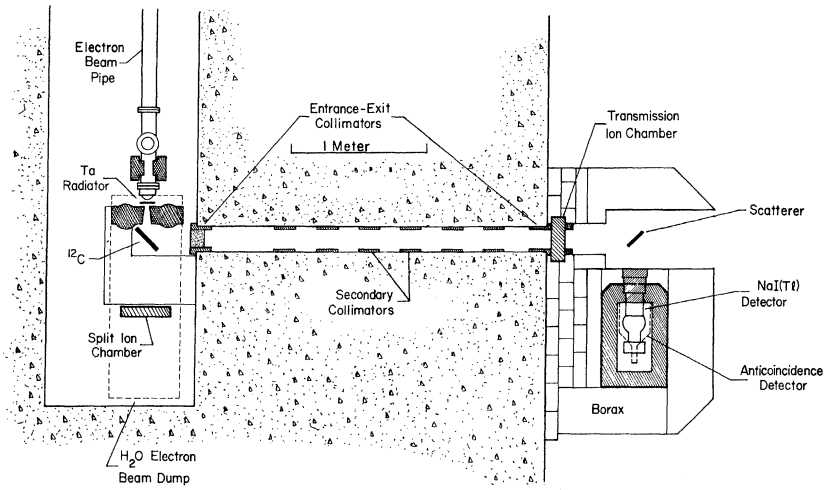


FIG. 1. Plan view of the experiment.

a second during a 5-$\mu$sec period around the 3-$\mu$sec-long beam burst.

The energy scale for the NaI(Tl) detectors was established using radioactive sources and checked routinely using the 4.43-MeV $\gamma$ ray emitted by a RaDBe source. The amplifier gains were adjusted so that the center of the full-energy 4.43-MeV peak fell in channel 48 of the 64-channel pulse-height analyzer. Then a 3.41 : 1 (3.41 = 15.1/4.43) attenuator was introduced into the system at the earliest convenient point, i.e., where the pulses came into the counting room. In this way 15.1-MeV pulses were registered at the same pulse size as the 4.43-MeV pulses in the calibration runs. This scheme was checked out using the pulse sizes produced by the 1.28-MeV $\gamma$ ray from a $^{22}$Na source with the 4.43-MeV pulse sizes (3.46 = 4.43/1.28).

During the initial phases of the experiment it became apparent that the true counting rate in the horizontal detector was comparable to its gated cosmic-ray background. Two plastic scintillators were therefore installed above the horizontal detector to serve as anticoincidence counters. Fortunately, there was room inside the lead casket to place one 20-×20-cm plastic scintillator just above the NaI(Tl) crystal, separated from it by 1.5 cm of plastic, and flush with the inside of the casket. A second plastic scintillator, 22×22 cm, was located above the casket overhanging the entrance surface of the NaI(Tl) detector. The outputs from these two counters were connected together, amplified, and passed through a discriminator that provided a standard pulse. When a true coincidence occured between either of the plastic scintillators and the horizontal NaI(Tl) detector, the pulse that gated the pulse-height analyzer on was cancelled. Pulse-height distributions for the horizontal detector were recorded both with and without this anticoincidence feature to be sure that the cosmic rays were being rejected at the appropriate rate. This arrangement eliminated about two thirds of the cosmic-ray background in the horizontal detector.

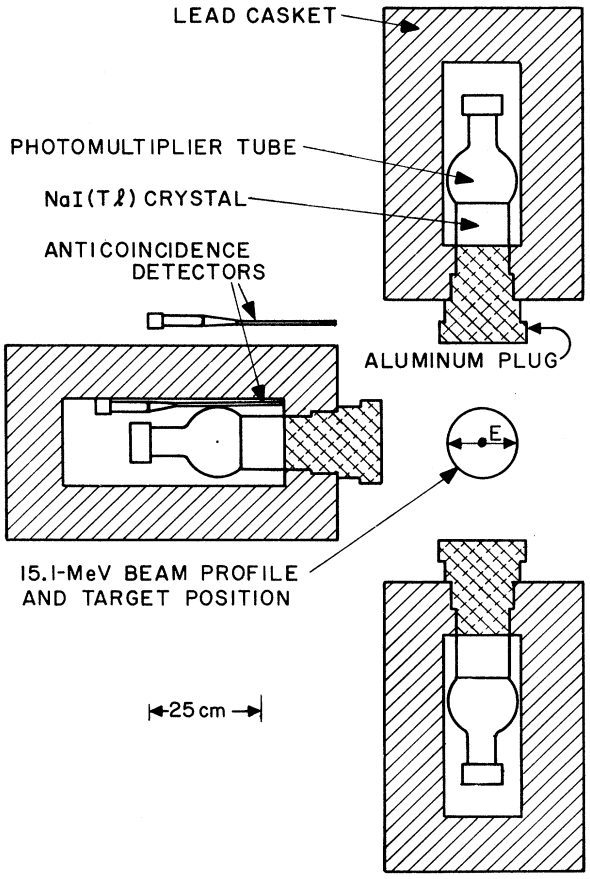


FIG. 2. The detector arrangement.

Cosmic-ray backgrounds were determined when the accelerator was off. First, the ungated background was measured for a short period, say, two hours. Then, the fully gated background using the anticoincidence feature on the horizontal detector was measured for a much longer period, say, 48 hours, with the pulse-height analyzers gated on at 1000 Hz using a pulser to simulate the accelerator pulse. These two pieces of data were then combined to obtain the appropriate backgrounds to be subtracted under the real experimental situation in which beam pulses occured at the rate 360 Hz. These were approximately 0.1 count/h for the horizontal detector and 0.3 count/h for each of the vertical ones.

In order to eliminate the accelerator-associated background it was necessary to surround the graphite target with boxes of borax. In addition, it was found helpful to provide a wall of borated polyethylene into which the horizontal detector looked.

The runs varied between 48 and 84 h. Usually, two targets were studied per run. The targets were exposed to the 15-MeV beam cyclically, first one target for two hours, the second for two hours, the target-out background for one hour, and then the sequence was repeated. The counting rate, uncorrected for backgrounds, was never more than 0.6 count/h in the horizontal detector and 3 counts/h in the veritcal ones.

The axes of the three detectors and the beam direction lie along the normals to a cube. If the targets are located in the plane defined by the body diagonals of this cube, then the target-detector geometry is the same for each of the three detectors. In this experiment the horizontal and lower detectors viewed the target in transmission

and the upper detector in reflection. In an idealized geometry the angles that the incident, reflected, and transmitted rays make with the normal to the target are all equal and equal to $\arccos 1/\sqrt{3} = 54°44'$.

The targets were smaller than the 18-cm beam dimension. The number of counts per monitor reading $C/M$ produced by a target having an area of $B$ cm$^2$ is

$$\frac{C}{MB} = f(\mu T)\,\frac{\Delta\Omega\epsilon}{\sigma_e}\,\frac{d\sigma}{d\Omega_F}. \tag{2.1}$$

This expression is written as an equality by sweeping the constant of proportionality into the monitor reading $M$. Here $\epsilon$ is the relative detector efficiency for which we have used the approximation, $\epsilon = 1 - e^{-\mu L}$, $L$ being the thickness of the sodium iodide crystal and $\mu$ its electronic absorption coefficient. The symbol $\sigma_e$ stands for the electronic absorption cross section in the target, essentially the sum of the pair-production and Compton-scattering cross sections, and $d\sigma/d\Omega_F$ is the photon-scattering cross section being studied. The subscript $F$ emphasizes that the detected photons are scattered only at approximately 90° because of the finite sizes of the detectors and targets. It will be denoted by $d\sigma^{\parallel}/d\Omega_F$ or $d\sigma^{\perp}/d\Omega_F$ according to whether it occurs parallel (horizontal) or perpendicular (vertical) to the polarization vector of the incident beam. The function $f(\mu T)$ takes into account the target thickness and the geometry, $\mu T$ being the number of mean free paths in the target. When the target is viewed in transmission

$$f_t(\mu T) = \sqrt{3}\,\mu T e^{-\sqrt{3}\mu T}, \tag{2.2}$$

and in reflection

$$f_r(\mu T) = \tfrac{1}{2}(1 - e^{-2\sqrt{3}\mu T}). \tag{2.3}$$

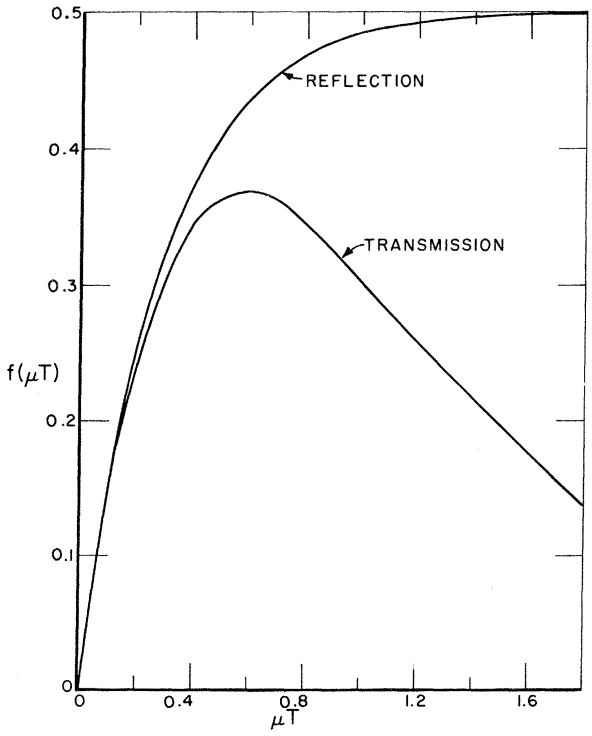


FIG. 3. A plot of the functions $f(\mu T)$ vs $\mu T$, Eqs. (2.2) and (2.3).

Figure 3 is a plot of $f(\mu T)$ as a function of $\mu T$. This shows that the optimum target thickness is $\mu T \sim 0.6$. Properties of the targets used in this experiment are given in Table I. Since lower-energy photons generated by Compton scattering or pair production followed by bremsstrahlung in the target are absorbed very strongly, it is preferable to view the target in transmission as do the horizontal and lower detectors.

## III. TREATMENT OF THE DATA

The quantities $C/M\epsilon f(\mu T)$ were evaluated for each target for each of the three detectors. The counts included were those in the 12-channel interval 41–52 which would include photons populating low-lying excited states up to about 3 MeV above the ground state. A pulse-height distribution produced in the upper detector by the photons scattered from the Pt target is shown in Fig. 4. The two arrows indicate the pulse-height interval taken for calculating scattered intensities. For the two vertical detectors the scattered intensities were always consistent. A weighted average was then obtained, for each target, including all the runs for the one horizontal and two vertical detectors. The errors were expressed as standard deviations based only on the number of counts.

A small correction was then made for the fact that the polarization of the 15.1-MeV beam was not perfect. This resulted from the angular spread of the bremsstrahlung when it stuck the carbon target which, in turn, was produced by the multiple scattering of the 20-MeV electrons prior to radiation in the 0.1-radiation-length-thick tantal-

TABLE I. Target properties.

| Target | $T$ (g/cm$^2$) | $\mu T$ | $f_t(\mu T)$ | $f_r(\mu T)$ | $B$ (cm$^2$) | $\sigma_e$ (b) |
|---|---|---|---|---|---|---|
| Cd | 12.56 | 0.525 | 0.3663 | 0.4189 | 232.3 | 7.91 |
| Sn | 12.77 | 0.566 | 0.3678 | 0.4296 | 232.3 | 8.37 |
| Ta | 12.83 | 0.667 | 0.3639 | 0.4504 | 232.3 | 15.63 |
| W | 12.19 | 0.639 | 0.3659 | 0.4453 | 232.3 | 16.00 |
| Pt | 11.14 | 0.602 | 0.3676 | 0.4379 | 232.3 | 17.20 |
| Au | 9.23 | 0.498 | 0.3641 | 0.4109 | 180.6 | 17.66 |
| Bi | 12.2 | 0.678 | 0.3629 | 0.4523 | 161.3 | 19.16 |

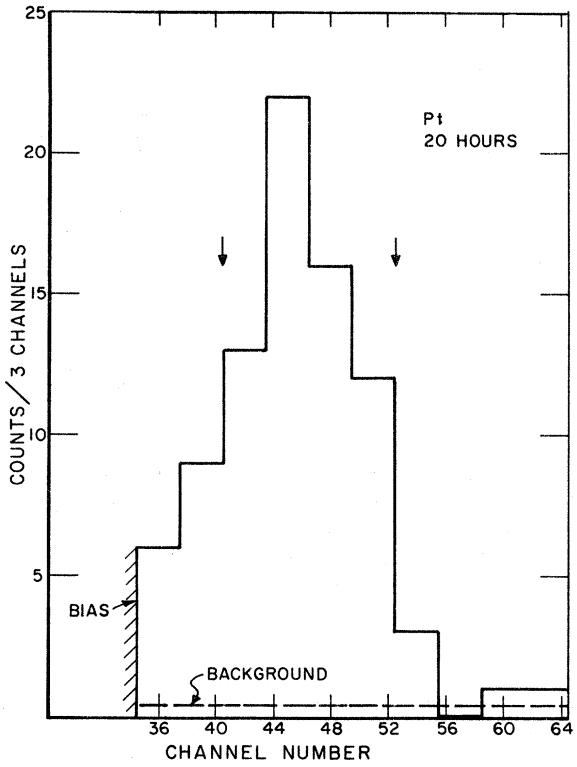


FIG. 4. The raw pulse-height distribution produced by 15.1-MeV plane-polarized photons scattered at 90° by the Pt target into the upper detector. The dashed line indicates the background level which for this run resulted only from cosmic rays. The arrows indicate the range of pulse height included in calculating relative cross sections.

um target. The polarization of the 15.1-MeV beam was estimated to be 95.8% using the angular distribution[18] of the 20-MeV thick-target bremsstrahlung. The contamination of the 15.1-MeV beam by scattering from the electric dipole giant resonance was estimated to be less than 1% and has been neglected. Had electron energies much greater than 20 MeV been used, the effects of electric dipole scattering would have been very serious.

After correction for the imperfect polarization of the 15.1-MeV beam, the quantities $C/M\epsilon f(\mu T)$ were multiplied by $\sigma_e/B$ to obtain $d\sigma^{\parallel}/d\Omega_F$ and $d\sigma^{\perp}/d\Omega_F$ according to Eq. (2.1) (see Table II). These are then relative cross sections since no attempt has been made to determine either the absolute number of photons incident on the targets nor the absolute detector efficiencies; the product $M\epsilon$ may be then viewed as an arbitrary constant that contains this normalization. The quoted errors are standard deviations based only on the number of counts. They are of the order of 30% for $d\sigma^{\parallel}/d\Omega_F$ and 10% for $d\sigma^{\perp}/d\Omega_F$ and are therefore large compared to a total estimated systematic error of 1%.

The general expression[19-21] for the nuclear electric dipole scattering cross section is

$$\frac{d\sigma}{d\Omega}=\sum_{\nu=0}^{2}\frac{|A_\nu|^2}{2\nu+1}g_\nu(\theta,\varphi), \tag{3.1}$$

where the $A_\nu$ are the scattering amplitudes associated with scattering in which $\nu=0, 1, 2$ units of angular momentum are taken up by the nucleus in the two-step scattering process. The $g_\nu(\theta,\varphi)$ are the angular-distribution factors; they depend on the angle between the polarization vectors of the incoming and outgoing photons, $\lambda$ and $\mu$:

$$\begin{aligned} g_0&=\tfrac{1}{3}(\lambda\cdot\mu)^2,\\ g_1&=\tfrac{1}{2}[1-(\lambda\cdot\mu)^2],\\ g_2&=\tfrac{1}{2}[1+\tfrac{1}{3}(\lambda\cdot\mu)^2]. \end{aligned} \tag{3.2}$$

If $\theta$ is the scattering angle and $\varphi$ the angle between $\lambda$ and the plane of scattering, then[21]

$$\begin{aligned} (\lambda\cdot\mu_1)&=\cos\theta\cos\varphi,\\ (\lambda\cdot\mu_2)&=\sin\varphi, \end{aligned} \tag{3.3}$$

where $\mu_1$ and $\mu_2$ are the two polarization vectors of the outgoing photon in and perpendicular to the plane of scattering. Summing over these two polarizations, we have

$$\begin{aligned} g_0&=\tfrac{1}{3}(\cos^2\theta\cos^2\varphi+\sin^2\varphi),\\ g_1&=1-\tfrac{1}{2}(\cos^2\theta\cos^2\varphi+\sin^2\varphi),\\ g_2&=1+\tfrac{1}{6}(\cos^2\theta\cos^2\varphi+\sin^2\varphi). \end{aligned}$$

TABLE II. Results.

| Target | $d\sigma^{\parallel}/d\Omega_F$ Arbitrary units | $d\sigma^{\perp}/d\Omega_F$ Arbitrary units | $\eta_F$ | $\eta$ | $\eta(DCM)$ |
|---|---|---|---|---|---|
| Cd | 0.042 ± 0.028 | 0.39 ± 0.05 | 0.11 ± 0.07 | 0.09 ± 0.07 | 0.19 |
| Sn | 0.084 ± 0.036 | 0.65 ± 0.06 | 0.13 ± 0.06 | 0.11 ± 0.06 | 0.07 |
| Ta | 0.24 ± 0.10 | 1.47 ± 0.14 | 0.16 ± 0.07 | 0.14 ± 0.07 | 0.20 |
| W | 0.52 ± 0.10 | 1.66 ± 0.12 | 0.31 ± 0.07 | 0.29 ± 0.07 | 0.20 |
| Pt | 0.23 ± 0.08 | 1.94 ± 0.13 | 0.12 ± 0.04 | 0.10 ± 0.04 | 0.08 |
| Au | 0.39 ± 0.11 | 2.08 ± 0.15 | 0.19 ± 0.06 | 0.17 ± 0.06 | 0.07 |
| Bi | 0.10 ± 0.15 | 2.65 ± 0.26 | 0.04 ± 0.06 | 0.02 ± 0.06 | 0 |

Since $A_1$ is negligible,[22] Eq. (3.1) simplifies to

$$d\sigma/d\Omega = |A_0|^2 g_0 + \tfrac{1}{5}|A_2|^2 g_2 . \tag{3.5}$$

For $\theta = \pi/2$ and $\varphi = 0$,

$$d\sigma^{\parallel}/d\Omega = \tfrac{1}{5}|A_2|^2 , \tag{3.6}$$

and for $\theta = \varphi = \pi/2$,

$$d\sigma^{\perp}/d\Omega = \tfrac{1}{3}|A_0|^2 + \tfrac{7}{30}|A_2|^2 . \tag{3.7}$$

Their ratio

$$\eta = \frac{d\sigma^{\parallel}/d\Omega}{d\sigma^{\perp}/d\Omega} = \frac{|A_2|^2/|A_0|^2}{\frac{5}{3} + \frac{7}{6}|A_2|^2/|A_0|^2} . \tag{3.8}$$

The ratio $\eta$ is plotted in Fig. 5 as a function of $|A_2|^2/|A_0|^2$.

Unfortunately, the target and detector are both finite in extent so that a photon can be scattered and detected at angles slightly different from $\theta = \pi/2$ and $\varphi = 0, \pi/2$. The ratio $\eta_F$ taking into account the sizes of the detectors and the various targets, has been calculated numerically for a series of values of $|A_2|^2/|A_0|^2$. The curve for the 15-×15-cm target is also shown in Fig. 5. For all practical purposes the measured value $\eta_F$ is increased by 0.02 over the point-target–point-detector value of $\eta$, almost independent of $|A_2|^2/|A_0|^2$. Experimentally determined values for $\eta_F$ and $\eta$ are given in Table II.

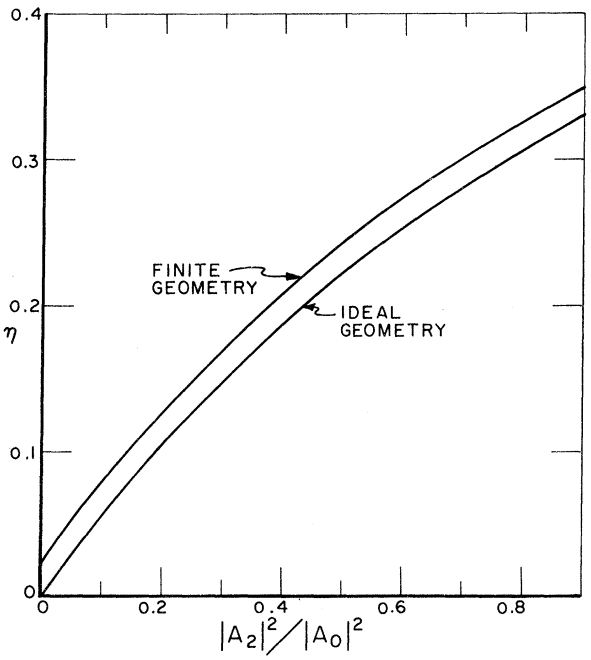


FIG. 5. The dependence of $\eta$ on $|A_2|^2/A_0|^2$. The lower curve is based on Eq. (3.8) while the upper one, which represents the actual experiment, was calculated numerically for the 15-×15-cm target taking into account the actual solid angles.

## IV. DISCUSSION

For purposes of discussion, we separate the available target nuclei into three classes: (1) rigid spheres, (2) deformed nuclei, and (3) spherical vibrators. The rigid sphere, exemplified by Bi, should have no tensor polarizability, hence, no inelastic scattering, and the counting rate in the horizontal detector should stem only from extraneous effects, i.e., cosmic-ray background, finite solid angle of the detector system, and contamination of the 15-MeV beam by photons having the wrong polarization. For the statically deformed nuclei, Ta or W, the tensor polarizability is large and well understood, and the incoherent scattering is dominated by that which populates those members of the ground-state rotational band that can be reached in electric dipole transitions. For the spherical vibrators, Cd, Sn, Au, and Pt, on the other hand, the tensor polarizability can only result from the coupling of the giant resonance with the quadrupole oscillations of the nuclear surface which, in turn, reflects its dynamic deformation. It was our purpose to observe this incoherent scattering in the horizontal detector and to obtain some measure of its intensity.

In the simple hydrodynamic model, which ignores the softness of the nuclear surface, the giant-resonance absorption and scattering cross sections are derived from the same complex forward-scattering amplitude.[20] For the spherical nuclei this is often represented by a Lorentz-shaped resonance line

$$R(E,0) = \frac{NZ\beta}{AMc^2} E^2 \frac{E_0^2 - E^2 + i\Gamma E}{E_0^2 - E^2 + \Gamma^2 E^2} , \tag{4.1}$$

where the symbol $\beta$ stands for the amount by which the integrated absorption cross section exceeds one electric dipole sum. By analogy, the forward-scattering amplitude for the permanently deformed nuclei is the sum of two Lorentz lines, the high-energy one having twice the area of the lower:

$$R(E,0) = \frac{A(E,0) + 2B(E,0)}{3} . \tag{4.2}$$

In this notation the coherent scattering cross section for unpolarized incident radiation is

$$\left(\frac{d\sigma}{d\Omega}\right)_0 = \left|\frac{A+2B}{3} + D\right|^2 \frac{(1+\cos^2\theta)}{2} , \tag{4.3}$$

where $D$ is the energy-independent nuclear Thomson scattering amplitude,

$$D = -\frac{Z^2 e^2}{AMc^2} . \tag{4.4}$$

The rigid rotators have additional incoherent com-

ponents in their scattering cross sections resulting from the transfer of two units of angular momentum to the nucleus ($\nu=2$). These components populate those members of the ground-state rotational band that can be reached in two electric dipole transitions

$$\left(\frac{d\sigma}{d\Omega}\right)_2 = |A-B|^2 \frac{(13+\cos^2\theta)}{90}. \tag{4.5}$$

A comparison of these equations with an expansion of Eq. (3.1)

$$\frac{d\sigma}{d\Omega} = |A_0|^2 \frac{(1+\cos^2\theta)}{6} + |A_2|^2 \frac{(13+\cos^2\theta)}{60} \tag{4.6}$$

leads to the relationship

$$|A_0|^2 = 3|R(E,0)|^2 = 3\left|\frac{A+2B}{3}+D\right|^2, \tag{4.7}$$

$$|A_2|^2 = \tfrac{2}{3}|A-B|^2. \tag{4.8}$$

Using the photoneutron-production cross sections obtained by the Saclay group,[23-25] $|A_0|^2$ and $|A_2|^2$ were evaluated for the deformed nuclei Ta and W. These were inserted into Eq. (3.8) to obtain the values of $\eta$ of 0.16 and 0.13, respectively, for Ta and W. The experimentally observed $\eta$ for Ta is certainly consistent with the rigid-rotator value whereas the observed $\eta$ for W is essentially twice as large. This result suggests that the nuclear surface for W is softer than for Ta and that the $\gamma$-vibrational band head is more strongly populated in the deexcitation of its giant resonance.

The positive values of $\eta$ given in Table II show that there is some incoherent scattering for all the targets studied except Bi. Values of $\eta$, calculated using the dynamic collective model,[26] are shown for comparison in the last column. These differ from those given in Ref. 17, since more realistic widths for the states that comprise the giant resonance have been used. For the spherical nuclei, all widths were taken to be 2.5 MeV whereas the formula $\Gamma_n = \Gamma_0(E_n/E_0)^\delta$ with $\Gamma_0 = 2.2$ MeV and $\delta = 1.6$ was used for the deformed nuclei W and Ta. Here, the $E_n$ are the energies of the giant resonance states and $E_0$ is the energy of the lower giant resonance peak. The value, $\eta = 0.08$, quoted for Pt, is the average value for $^{194}$Pt, $^{196}$Pt, and $^{198}$Pt weighted according to their abundances. The value quoted for Au is that for $^{196}$Pt, since according to the weak-coupling model,[17] the addition of a proton to $^{196}$Pt only splits the energy levels and redistributes the strength. Apparently, the incoherent scattering from gold is somewhat stronger than this prediction. The results of this experiment, though crude, generally agree with the predictions of the dynamic collective model. If anything, there is too much incoherent scattering from gold and especially tungsten. In any case, a coupling between the low-lying vibrational states and the giant resonance is evident.

As a check on the over-all consistency of these results, i.e., $Z$ dependence, they have been compared with the photoneutron-production cross sections measured by the Saclay group[23-25] for the same targets. From the scattering experiment a quantity proportional to $|A_0|^2$ can be obtained from the relationship

$$|A_0|^2 \sim d\sigma^\perp/d\Omega - \tfrac{7}{6}d\sigma^\parallel/d\Omega. \tag{4.9}$$

The quantity $|A_0|^2$ has also been calculated from the Saclay cross sections by making use of Eq. (4.7).

This comparison is summarized in Table III where the data of Table II have been combined according to Eq. (4.9) to yield a quantity proportional to $|A_0|^2$. The results obtained from the Saclay data are given in the third column. The ratio of these two quantities which should be a constant is tabulated in the last column. The agreement is quite satisfactory.

There are several other phenomena, so far ignored, which may influence these results: (1) Delbrück scattering; (2) scattering from continuum levels with parity opposite to the electric dipole; and (3) coherent scattering resulting from a scalar polarizability not associated with the hydrodynamic model. Now a few words about each of these in turn.

Delbrück scattering is the coherent-scattering process, associated with pair production, which can, in principle, interfere with the nuclear coherent scattering. This process is peaked very strongly forward and varies as $Z^4$. Estimates of $d\sigma^\parallel/d\Omega(\pi/2)$ and $d\sigma^\perp/d\Omega(\pi/2)$ were made for Bi, the heaviest target studied here, including the nuclear Thomson scattering, the nuclear resonance scattering, and the Delbrück scattering amplitudes. The nuclear-scattering amplitudes were based on the Lorentz line parameters for Pb given in Ref.

TABLE III. Comparison with Saclay data.

| | $\lvert A_0\rvert^2$ This experiment (arb. units) | $\lvert A_0\rvert^2$ Saclay (mb) | Ratio |
|---|---|---|---|
| Cd | 0.337 ± 0.058 | 0.508 | 0.663 ± 0.114 |
| Sn | 0.550 ± 0.072 | 0.822 | 0.669 ± 0.088 |
| Ta | 1.19 ± 0.18 | 1.88 | 0.633 ± 0.096 |
| W | 1.05 ± 0.17 | 2.05 | 0.512 ± 0.083 |
| Pt | 1.67 ± 0.16 | 2.70 | 0.619 ± 0.059 |
| Au | 1.62 ± 0.20 | 2.92 | 0.555 ± 0.068 |
| Bi | 2.53 ± 0.31 | 3.43 | 0.737 ± 0.090 |
| | | | 0.616 ± 0.030 |

25, and the Delbrück scattering amplitudes were obtained by interpolation of the amplitudes given by Ehlotzky and Sheppey.[27] It transpires that Delbrück scattering does permit some scattering along the polarization vector at 90° so that the calculated ratio becomes $\eta = 0.01$. In view of the statistical errors involved in this experiment, this effect does not represent an important contamination.

There is no real evidence for it, but if there were at 15.1 MeV strong $2^+$ or $1^+$ states superimposed on the giant resonance $1^-$ states, 15.1-MeV photons could be scattered along the polarization vector into the horizontal detector.

There is some evidence[2,28,29] that the nuclear polarizability has a nonresonant[30] part that is not described by the hydrodynamic model nor by its refinement, the dynamic collective model. This part of the polarizability is a scalar related to the absorption cross section and the coherent-scattering cross section. A recent experiment[31] indicates that it may be large enough to increase $|A_0|^2$ by 30%, thus making the ratio $\eta$ more difficult to measure. Because of the structure of Eq. (3.8), such an increase in $|A_0|^2$ appears as a decrease of only 12% in $\eta$.

## ACKNOWLEDGMENTS

The authors wish to thank Dr. H. Arenhövel for providing the results given in the last column of Table II and Dr. R. Bergère and Dr. A. Veyssière for sending the unpublished Saclay data that form the basis of the comparison made in Table III. They also thank Dr. S. Penner and the staff of the National Bureau of Standards linear accelerator for help without which this experiment could never have gone forward.

## APPENDIX: RELATIONSHIP TO THE REORIENTATION EXPERIMENTS

Eichler[32] has pointed out that second-order transitions through the giant resonance can be important to the reorientation effect in Coulomb excitation. The correction is proportional to the ratio of the polarizabilities.

$$\eta = \frac{\sum_n \langle 0^+|Z|n\rangle\langle n|Z|2^+\rangle/E_n}{\sum_n \langle 0|Z|n\rangle\langle n|Z|0^+\rangle/E_n}.$$

For strongly deformed nuclei this expression takes on an especially simple form[33,34] in the simple two-resonance model

$$\eta = \frac{2}{\sqrt{5}}\left(\frac{E_b^2 - E_a^2}{E_b^2 + 2E_a^2}\right).$$

Here $E_a$ is the energy of the lower resonance which contains one third of the strength and $E_b$ is the energy of the upper one having two thirds of the strength. When evaluated for the very deformed nuclei, Ho or Er, $\eta = 0.19$.

For the spherical vibrators the coupling between the giant-dipole state and the $2^+$ state can be calculated in the dynamic collective model. Douglas and MacDonald[34] have given a simple formula in terms of the model parameters which yield values of Eichler's $\eta$ for these nuclei in the range 0.10 to 0.15.

The ratio of scattering cross sections $\eta$ obtained in the present experiment is not the same as Eichler's $\eta$ but is related to it. A nonzero value for either one for a spherical nucleus represents a coupling between the dipole state and the $2^+$ state and they can both be estimated in the same model. Two distinctions need to be made. Eichler's $\eta$ is the ratio of polarizabilities, the numerator being related to $A_2$ and the denominator to $A_0$. Our $\eta$ is the ratio of scattering cross sections, the numerator being $|A_2|^2$ and the denominator a linear combination of $|A_0|^2$ and $|A_2|^2$. Eichler's $\eta$ involves the sum over all electric dipole transitions $n$, ours only those contributing within the width of the 15.1-MeV line which is near the center of the giant resonance for the nuclei studied. Nevertheless, the fact that we have a positive result, however crude, consistent with the dynamic collective model, supports the use of that same model to determine the corrections to the reorientation effect.

It has recently been reported[35] in connection with reorientation experiments on light nuclei that the coupling between the giant dipole and $2^+$ states is much more important. This implies that the transition from the giant resonance to the $2^+$ state would be relatively much more intense than it is for the nuclei studied here. An experimental measurement of these branching ratios would require monochromatic photons of energies higher than 15 MeV to reach the giant resonances of light nuclei. On the other hand, a polarized beam may not be required, since the final states are more widely separated so that the elastic and inelastic components in the scattered radiation might be separated spectroscopically.

---

*Work supported by the U. S. Atomic Energy Commission under Contract No. AT(11-1)-3069 and guest worker at the National Bureau of Standards.

†Harry Diamond Laboratories Fellow at The American University and guest worker at the National Bureau of Standards. The material contained herein was submit-

ted in partial fulfillment of the requirements for the Ph.D. degree in the Department of Physics, The American University, Washington, D. C.
[1]E. G. Fuller and E. Hayward, Phys. Rev. Lett. 1, 465 (1958).
[2]E. G. Fuller and E. Hayward, Nucl. Phys. 30, 613 (1962).
[3]P. A. Tipler, P. Axel, N. Stein, and D C. Sutton, Phys. Rev. 129, 2096 (1963).
[4]M. Danos and W. Greiner, Phys. Rev. 134, B284 (1964).
[5]J. Le Tourneux, Phys. Lett. 13, 325 (1964).
[6]J. Le Tourneux, K. Dan. Vid. Selsk. Mat.-Fys. Medd. 34, No.11 (1965).
[7]S. F. Semenko, Phys. Lett. 10, 182 (1964); 13, 157 (1964).
[8]S. F. Semenko, Yad. Fiz. 1, 414 (1965) [transl.: Sov. J. Nucl. Phys. 1, 295 (1965)].
[9]A. K. Kerman and H. K. Quang, Phys. Rev. 135, B883 (1964).
[10]D. S. Fielder, J. Le Tourneux, K. Min, and W. D. Whitehead, Phys. Rev. Lett. 15, 33 (1965).
[11]P. H. Cannington, R. S. S. Stewart, B. M. Spicer, and M. G. Huber, Nucl. Phys. A109, 385 (1968).
[12]D. G. Owen, E. G. Muirhead, and B. M. Spicer, Nucl. Phys. A122, 177 (1968).
[13]O. V. Vasilijev, G. N. Zalesny, S. F. Semenko, and V. A. Semenov, Phys. Lett. 30B, 97 (1969).
[14]S. F. Semenko, O. V. Vasilijev, and V. A. Semenov, Phys. Lett. 31B, 429 (1970).
[15]M. Danos and E. G. Fuller, Ann. Rev. Nucl. Sci. 15, 29 (1965).
[16]H. Arenhövel and J. M. Maison, Nucl. Phys. A147, 305 (1970).
[17]H. Arenhövel and E. Hayward, Phys. Rev. 165, 1170 (1968).
[18]M. J. Berger and S. M. Seltzer, Phys. Rev. C 2, 621 (1970).
[19]E. Hayward, in *Nuclear Structure and Electromagnetic Interactions*, edited by N. MacDonald (Oliver & Boyd, Edinburgh, Scotland, 1965).
[20]E. Hayward, National Bureau of Standards Monograph No. 118 (U. S. GPO, Washington, D. C., 1970).
[21]U. Fano, National Bureau of Standards Technical Note No. 83 (U. S. GPO, Washington, D. C., 1960).
[22]E. G. Fuller and E. Hayward, *Nuclear Reactions II*, edited by P. M. Endt and P. B. Smith (North-Holland, Amsterdam, 1962).
[23]R. Bergère, H. Beil, and A. Veyssière, Nucl. Phys. A121, 463 (1968).
[24]A. Veyssière, H. Beil, R. Bergère, P. Carlos, and A. Lepetre, Nucl. Phys. A159, 561 (1970).
[25]R. Bergère and A. Veyssière, private communication.
[26]H. Arenhövel, private communication.
[27]F. Ehlotzky and G. C. Sheppey, Nuovo Cimento 33, 1185 (1964).
[28]E. Ambler, E. G. Fuller, and H. Marshak, Phys. Rev. 138, B117 (1965).
[29]M. A. Kelley, B. L. Berman, R. L. Bramblett, and S. C. Fultz, Phys. Rev. 179, 1194 (1969).
[30]H. Arenhövel, Phys. Rev. C 6, 1449 (1972).
[31]H. E. Jackson and K. J. Wetzel, Phys. Rev. Lett. 28, 513 (1972).
[32]J. Eichler, Phys. Rev. 133, B1162 (1964).
[33]N. MacDonald, Phys. Lett. 10, 334 (1964).
[34]A. C. Douglas and N. MacDonald, Phys. Lett. 24B, 447 (1967).
[35]O. Häusser, in Proceedings of the International Conference on Nuclear Moments and Nuclear Structure, September 1972 (to be published).